Supporting Information for

Computational discovery of In_2XY_2 (X, Y= S, Se and Te; X ≠ Y) monolayers as multifunctional energy conversion materials

Rui Xiong[1], Weiqiang Li[1], Yinggan Zhang[2], Zhou Cui[1], Cuilian Wen[1], Masakazu Anpo[3], Bo Wu[1], and Baisheng Sa[1,*]

[1]*Key Laboratory of Eco-materials Advanced Technology, College of Materials Science and Engineering, Fuzhou University, Fuzhou 350108, P. R. China*

[2] *College of Materials, Fujian Provincial Key Laboratory of Theoretical and Computational Chemistry, Xiamen University, Xiamen 361005, P. R. China*

[3] *State Key Laboratory of Photocatalysis on Energy and Environment, Fuzhou University, Fuzhou 350116, P. R. China*

Corresponding Author: *bssa@fzu.edu.cn (B. Sa)

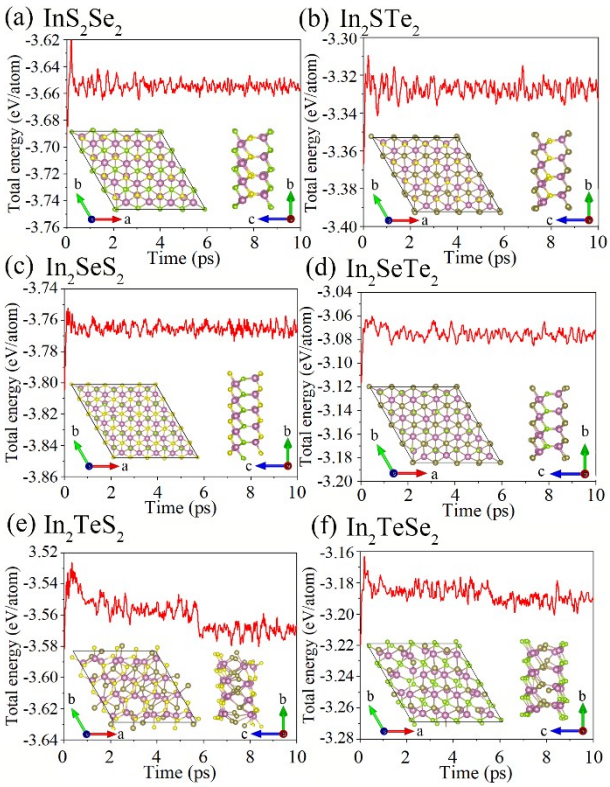

Figure S1. The evolution of total energy and snapshot structure from AIMD simulations of (a) In_2SSe_2, (b) In_2STe_2, (c) In_2SeS_2, (d) In_2SeTe_2, (e) In_2TeS_2, (f) In_2TeSe_2 for 10 ps at 300 K.

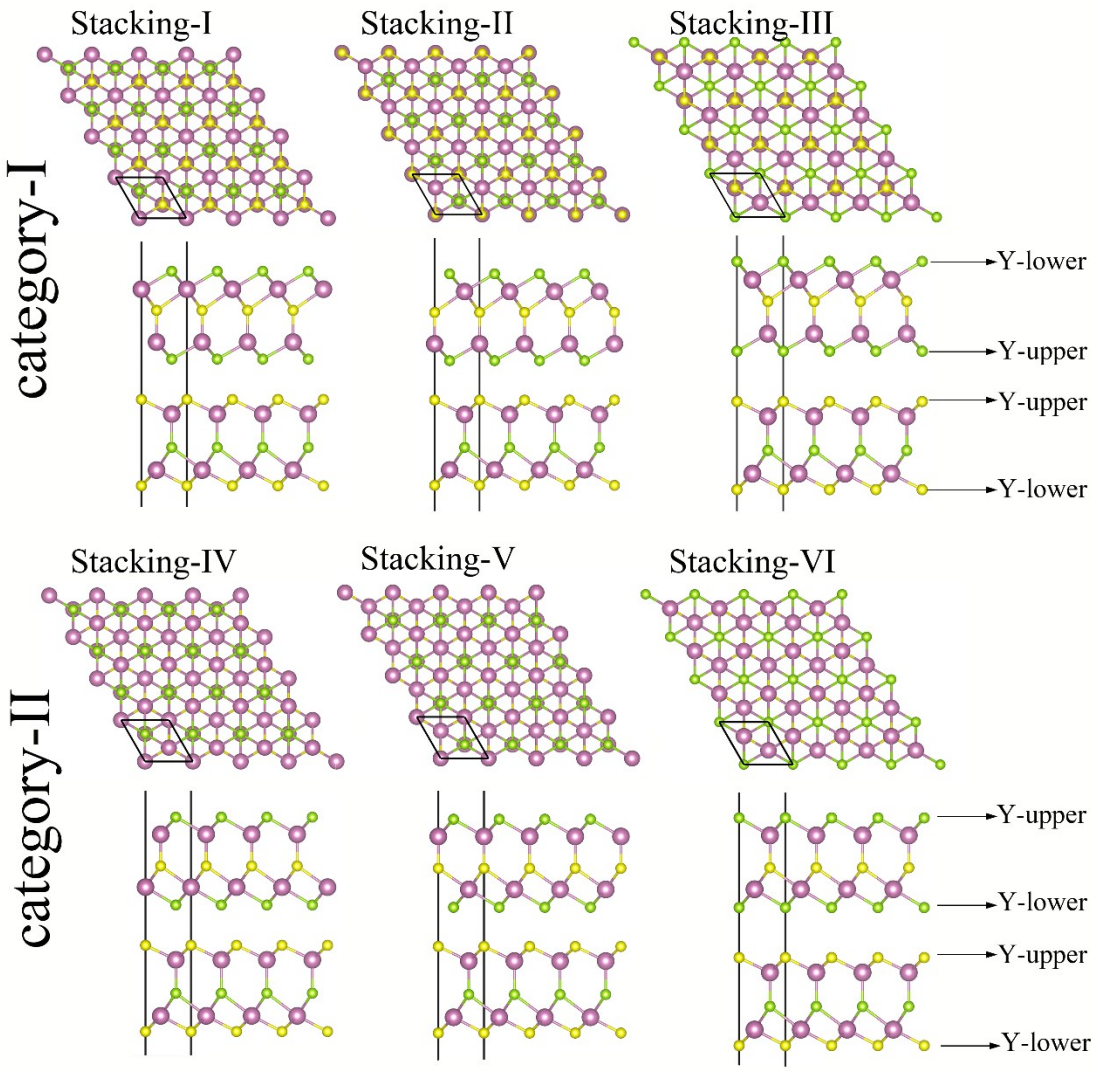

Figure S2. The six stacking configurations of In_2SSe_2/In_2SeS_2 and In_2STe_2/In_2SeTe_2 heterostructures.

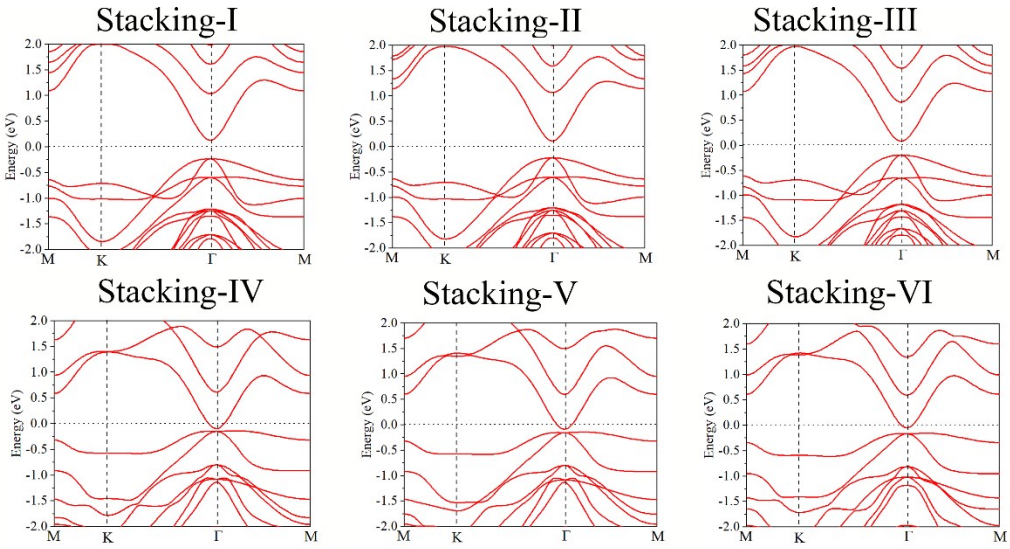

Figure S3. The band structures of In_2SSe_2/In_2SeS_2 heterostructure with different stacking configurations using PBE functional.

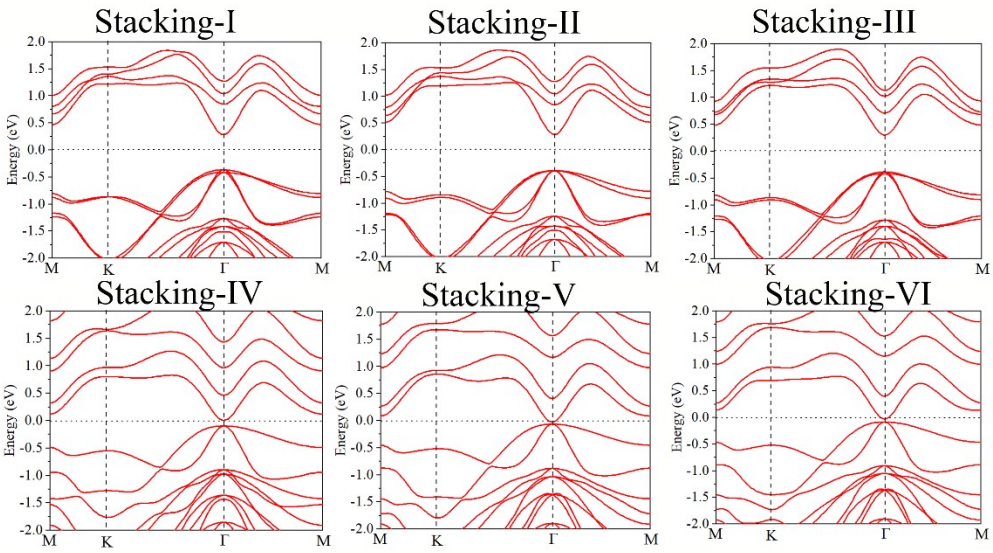

Figure S4. The band structures of In_2STe_2/In_2SeTe_2 heterostructure with different stacking configurations using PBE functional.

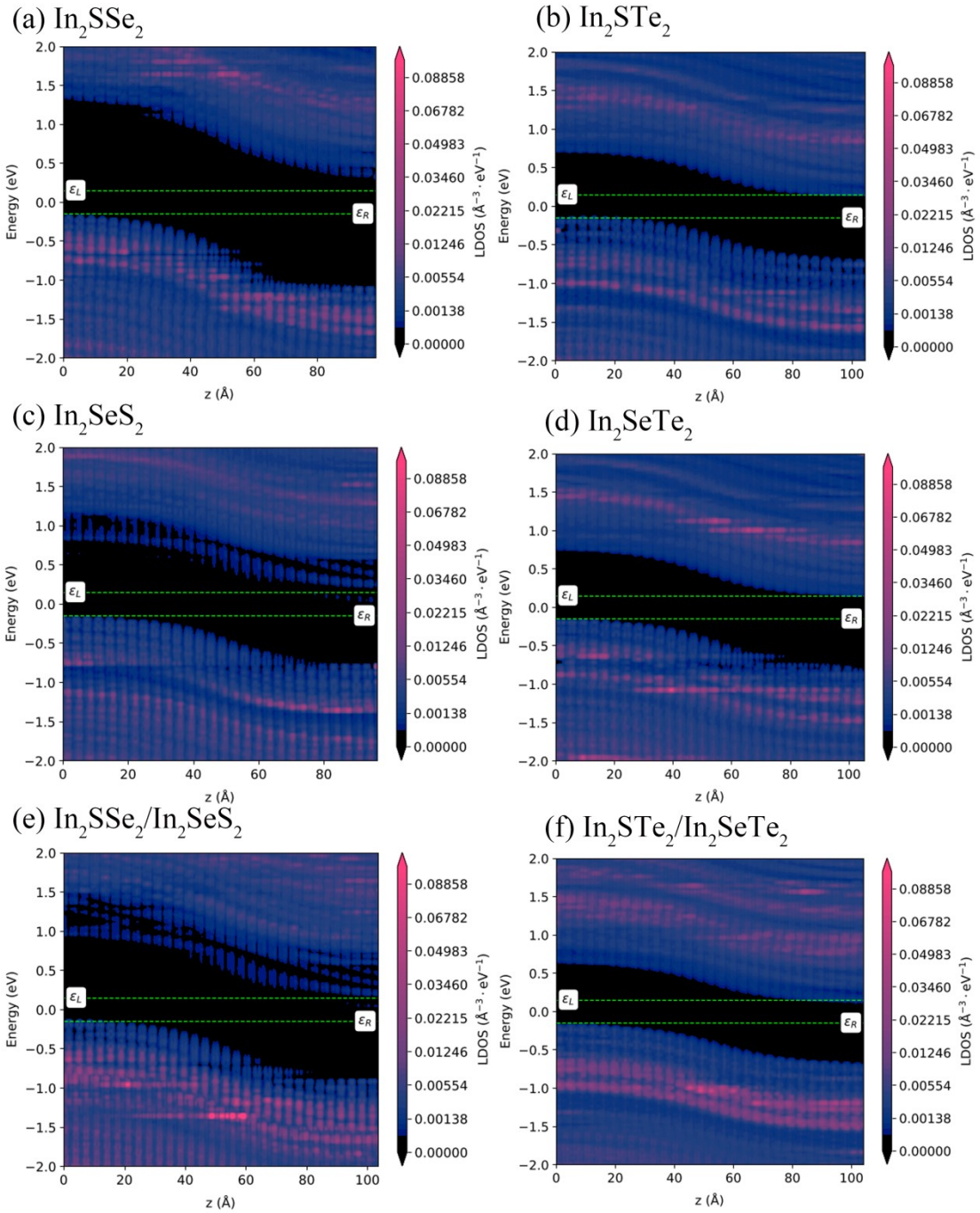

Figure S5 The local density of states (LDOS) of solar cell devices (a) $InSSe_2$, (b) $InSTe_2$, (c) $InSeS_2$, (d) $InSeTe_2$, (e) $InSSe_2/In_2SeS_2$ and (f) $InSTe_2/In_2SeTe_2$.

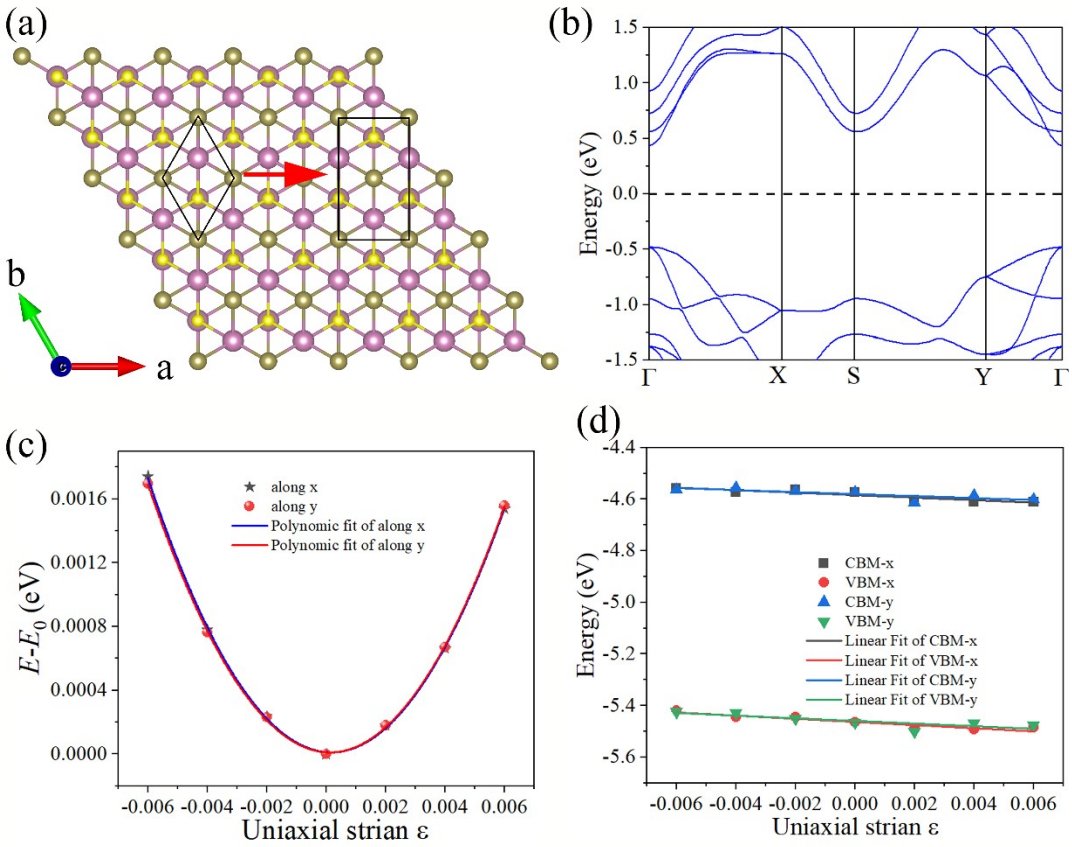

Figure. S6. (a) In_2STe_2 monolayer in an orthorhombic lattice instead of a hexagonal lattice. (b) Band structure, (c) total energy shift ($E - E_0$) and (d) band edge positions of In_2STe_2 monolayer as a function of the uniaxial strain ε along both the zigzag (x) and armchair (y) directions by PBE. The vacuum level is set to 0 for reference in (d).

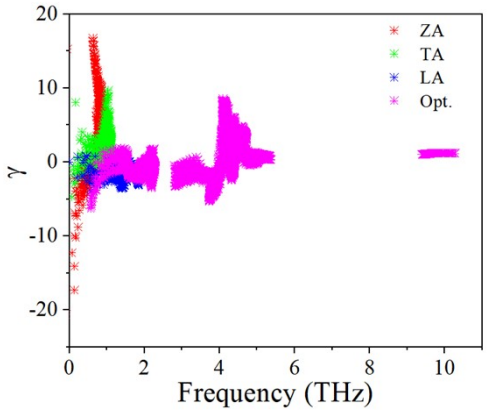

Figure S7. The calculated Grüneisen parameter γ as a function of phonon frequency for In_2STe_2 monolayer.

Table S1. The bonding length of In_2XY_2 and In_2X_3 monolayers

	L_{In1-X} (Å)	L_{In2-X} (Å)	$L_{In1-Y-upper}$ (Å)	$L_{In2-Y-lower}$ (Å)
In_2SSe_2	2.83	2.42	2.69	2.66
In_2STe_2	2.91	2.42	2.89	2.85
In_2SeS_2	2.87	2.54	2.59	2.55
In_2SeTe_2	2.98	2.56	2.91	2.87
In_2TeS_2	3.04	2.76	2.61	2.57
In_2TeSe_2	3.06	2.75	2.74	2.70
In_2S_3	2.79	2.41	2.57	2.41
In_2Se_3	2.91	2.55	2.71	2.68
In_2Te_3	3.11	2.76	2.94	2.88

Table S2. Calculated Effective Mass (m*), Elastic Modulid (C_{2D}), Deformation Potentials (E_l), and Carrier Mobility (μ) of In_2XY_2 monolayer along x and y directions

Direction	Carrier type	E_1(eV)	C_{2D} (N m^{-1})	m^*/m_0	μ(cm^2 V^{-1} s^{-1})	t(ps)
x	e	4.860	45.7	0.17	941.10	0.10
	h	6.110	45.7	1.61	6.60	0.01
y	e	3.910	45.4	0.17	1377.70	0.15
	h	5.110	45.4	1.75	8.00	0.01